

SOLAR POWERED MULTIPURPOSE REMOTELY POWERED AIRCRAFT

WORCESTER POLYTECHNIC INSTITUTE

5,0-05
160586
P-6

Environmental problems such as the depletion of the ozone layer and air pollution demand a change in traditional means of propulsion that is sensitive to the ecology. Solar-powered propulsion is a favorable alternative that is both ecologically harmless as well as cost effective. Integration of solar energy into designs ranging from futuristic vehicles to heating is, therefore, beneficial to society. The design and construction of a Multipurpose Remotely Piloted Vehicle (MPRPV) seeks to verify the feasibility of using solar propulsion as a primary fuel source. This task has been a year-long effort by a group of eight students, divided into four teams, each dealing with different aspects of the design.

The aircraft has been designed to take off, climb to the design altitude, fly in a sustained figure-eight flight path, and cruise for approximately one hour. This mission requires flight at Reynolds numbers between 150,000 and 200,000 and demands special considerations in the aerodynamic design to achieve flight in this regime. Optimal performance requires a lightweight configuration with both structural integrity and maximum power availability. The structural design and choice of solar cells for the propulsion were governed by weight, efficiency, and cost considerations.

The final design is an MPRPV weighing 35 N that cruises at 7 m/s at the design altitude of 50 m. The configuration includes a wing composed of balsa and foam NACA 6409 airfoil sections and carbon fiber spars, a tail of similar construction, and a truss structure fuselage. The propulsion system consists of 98 12.5%-efficient solar cells donated by Mobil Solar, a NiCad battery for energy storage, and a folding propeller regulated by a lightweight and efficient control system. The airfoils and propeller chosen for the design have been researched and tested during the design process.

aircraft to remain within a reasonable distance from the ground control. Once at altitude, a sustained figure-eight pattern tests the aircraft characteristics over a variety of maneuvers.

Aircraft Configuration

The proposed vehicle is shown in Figs. 1 and 2. General data and design parameters are summarized in Table 1.

The configuration consists of a nonconventional, high-wing aircraft with two carbon fiber composite support struts primarily important in maintaining structural integrity. The two composite

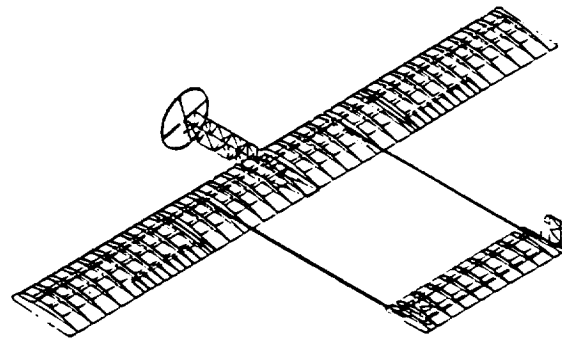


Fig. 1. Final design—Isometric view.

INTRODUCTION

Mission Requirements

This study investigates the possibilities for a remotely controlled solar-powered aircraft. Ultimately the aircraft will be able to perform a sustained figure-eight flight pattern at an altitude of 50 m using only solar power. The mission will be carried out in several flight stages including launch, climb to altitude, and pattern flight.

The aircraft will be launched away from the Sun employing a catapult system to provide some initial altitude. Maximum power will be received when the aircraft is traveling away from the Sun, resulting from the incidence of the solar array with respect to the Sun. Therefore the best climb rate will be achieved when flying in this direction. A circular climbing pattern will be used, to compensate for slow climb rates and enable the

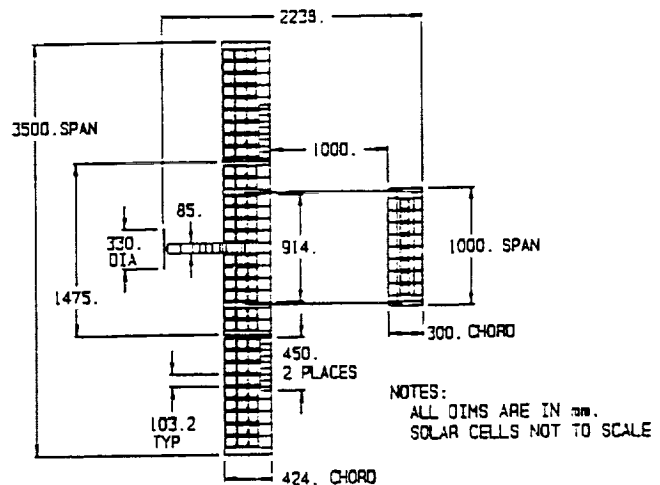


Fig. 2. Final design—Top view.

TABLE 1. General data.

Weight	W_{gross}	40 N
Wing Area	S	1.48 m ²
Wing Loading	W	27.03 N/m ²
Aspect Ratio	AR	8.25
Wingspan	b	3.5 m
Cruise Altitude	h	50 m
Cruise Velocity	V	7 m/s
Design Lift Coeff	C_L	0.83
Design Lift-to-Drag	L/D	15.75
Cruise Power Req'd	P	15.9 W
Design Load Factor	n	7

rods extend from the main spar in the wing to the spar of the horizontal stabilizer. This becomes of primary importance during both takeoff and landing, as large wing tip deflections could result in catastrophic failure.

A solar propulsion system, which includes 98 photovoltaic solar cells supplied by Mobil Solar Corporation, powers the aircraft. The cells directly power an Astro-Flight Cobalt 0.05 motor that drives a folding Aero-Haute 13 × 6.5" pitch plastic propeller. As a safety feature, a switch is included to provide access to a NiCad battery backup system.

The electronics equipment is housed in a small fuselage, connected to the underside of the main wing. The fuselage was built using a balsa truss structure covered with a mylar coating. The truss structure provided the fuselage with the necessary strength to safely house the electronics equipment under all anticipated loads, while minimizing the weight.

The wing and horizontal tail both have a prismatic planform with aerodynamic characteristics of NACA 6409 airfoil sections. The wing has a span of 3.5 m and a chord of 0.424 m, resulting in an aspect ratio of 8.25. The wing is attached to the fuselage at an angle of attack of 4°. At level flight conditions, this angle of attack produces a total wing C_L of 0.72 and downwash of -2°. The tail has a span of 1 m and chord of 0.3 m, resulting in an aspect ratio of 3.33. The C_L of the tail is 0.22 and efficiency assumed is 85%. The design at level flight conditions has an airplane lift coefficient of 0.83 and drag coefficient of 0.053 resulting in a configurational lift-to-drag ratio of 15.75.

In addition, the aircraft is equipped with a variety of control devices including two ailerons, two rudders, and an elevator. These are directed with an onboard receiver that uses four electronic servos to control their motion.

DESIGN AND ANALYSIS

Aircraft Sizing and Weight Estimation

The required mission mandates the proposed vehicle be powered solely by the Sun; therefore, the design was optimized for maximum power and minimum weight. A model aircraft provided by a kit was constructed and flown. This aircraft was not solar powered, but did provide a reasonable initial weight estimation and power requirement for the proposed solar-powered vehicle. Solar propulsion was integrated into the design and the configuration was iteratively improved until a final and unique vehicle was obtained. Tables 2 through 5 break down

TABLE 2. Wing component masses.

Wing	Parts	Mass (g)	% Wing
Ribs	30	99.2	4.8
Leading Edge	1	84.2	4.1
Trailing Edge	1	104.4	5.1
Spar Webs	33	44.8	2.2
Skin (Mylar)		192.9	9.3
Solar Braces (foam)	270	33.7	1.6
Wing Tips (foam)	2	36.1	1.7
Carbon Rods	2	91.0	4.4
Solar Cells	90	856.8	41.5
Servos	2	43.0	2.1
Wiring		55.1	2.7
Reinforcing Rib	10	340.0	16.5
Fasteners	10	82.2	4.0
Wing Total		2063	100

TABLE 3. Fuselage component masses.

Fuselage	Mass (g)	% Fuselage
Balsa Frame	111.6	12.5
Skin (Mylar)	12.3	2.5
Servo	21.5	2.4
Wiring	37.9	4.2
Motor & Gearbox	225.7	25.3
Propeller	32.9	3.7
Receiver Battery	97.0	10.9
Receiver	44.0	4.9
Speed Control	54.8	6.1
On/Off Switch	10.3	1.2
Emergency Batteries	234.3	26.2
Landing Gear	23.6	2.6
Fuselage Total	905.9	100

TABLE 4. Tubular strut masses.

Tail Strut	Mass (g)	% Strut
Carbon Tubes (2)	225.1	80.9
Wiring	53.2	19.1
Strut Total	278.3	100

TABLE 5. Tail component masses.

Tail	Parts	Mass (g)	% Tail
Ribs	9	14.2	4.5
Leading Edge	1	20.0	6.422
Spar Webs	9	6.4	2.0
Elevator	1	34.8	10.8
Skin (Mylar)		42.0	13.4
Solar Braces (foam)	16	2.0	0.6
Carbon Rods	2	2.6	0.8
Solar Cells	8	76.2	24.3
Vertical Tail	2	20.2	6.4
Servos	2	43.0	13.7
Reinforcing Rib	2	21.6	6.9
Fasteners	2	31.2	10.0
Tail Total		313.4	100

the actual masses for individual elements of the plane and also show the percent contribution of each to its element section of the plane.

Aerodynamic Design and Analysis

The wing has been designed to have a span of 3.5 m and a chord length of 0.424 m from its root to wing tip. A prismatic planform was selected to achieve the maximum amount of power per wing area. The flight regime corresponding to a Reynolds number of approximately 200,000 involves difficulty with viscous effects associated with the boundary layer and prediction of laminar separation bubbles. The computational methods at our disposal have proven inaccurate due to the physics of the flow. Reliable experimental data were obtained from *Soartech 8: Airfoils at Low Speeds*⁽¹⁾. Three airfoil sections were considered and their lift-to-drag ratios vs. angle of attack are shown in Fig. 3. The NACA 6409 was determined to be well suited to thermal sailplane gliding due to its aerodynamic performance at the design point. This airfoil has a maximum of 9% thickness and 6% camber both located at 40% chord and generates a C_L of 0.72 at level flight with an attack angle of 4°. Using the Eppler code⁽²⁾ the inviscid distribution of pressure for an angle of attack of 4° was determined.

The tail is similarly designed with the aerodynamic shape of the NACA 6409 and a prismatic planform of dimensions 0.3 m (chord length) × 1 m (span). This component has an angle of attack of 0° and generates a C_L of 0.2206 at level flight. Tail efficiency is assumed to be 85%.

The effects of finite wing length on the two-dimensional lift and drag curves were investigated using a Fourier series representation developed by Glauert (1937). The prismatic wing

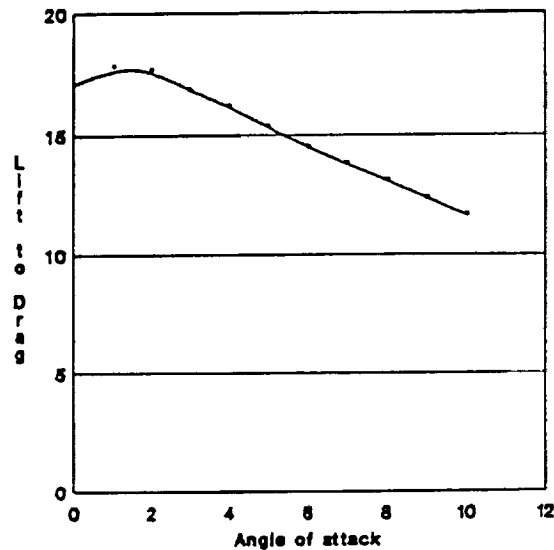


Fig. 4. Configurational lift-to-drag curve.

design of this aircraft deviates from the elliptic wing resulting in a 4% loss in lift and an 8% increase in drag. Twist and taper of the wing could alleviate these problems, yet these options were not implemented due to construction difficulties.

To determine the optimum operational point for the given configuration, a study of the variation of excess power with attack angle was administered. An attack angle of 4° was chosen corresponding to a trimmed tail at -2° (an angle of attack of 0° corresponding to the horizontal). The configurational lift-to-drag curve resulting from this study is shown in Fig. 4.

Structural Design and Analysis

This configuration employs a semimonocoque (stressed skin) structure composed of a balsa skeleton with a transparent mylar skin covering, providing a lightweight aerodynamic frame. Carbon fiber rods running the span of the wing and tail are the major strengthening elements in the wing and tail design. This spanwise spar consists of a 3.3-mm-diameter carbon fiber rod joined by balsa spar webs to create an I-beam structure. Structural half-models were created and analyzed using a professional version of ANSYS. Increasing levels of detail were incorporated during the course of the academic year.

Applying the maximum anticipated load (equivalent to a gust-induced aerodynamic lift of seven times the aircraft weight, simulating the design load factor) resulted in compressive and tensile stresses within the structure much less than those allowable for each component given its material properties. The maximum deflection and angle of twist in the wing are 0.24 m and 11.5° respectively, occurring in the wing tips. The tail is restrained at its tips by the connections to the carbon fiber supports and experiences a maximum deflection of only 0.515 mm at its midspan. The results of the ANSYS analysis substantiates the material selection and structural design by verifying the structure will not fail under the greatest anticipated loading.

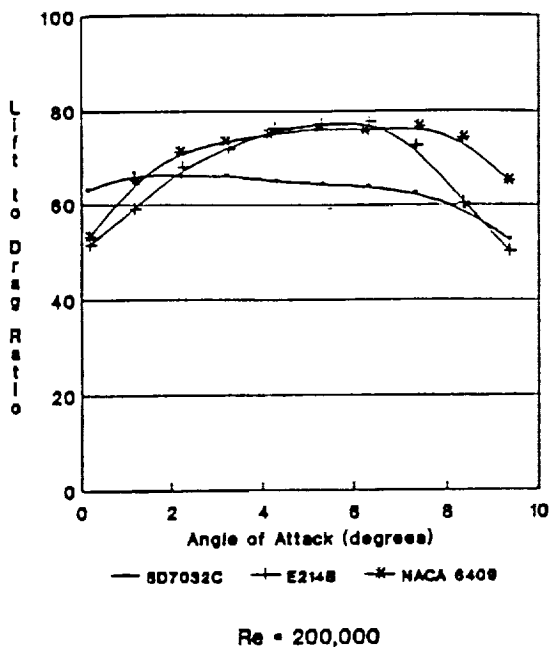


Fig. 3. Comparison of airfoil sections.

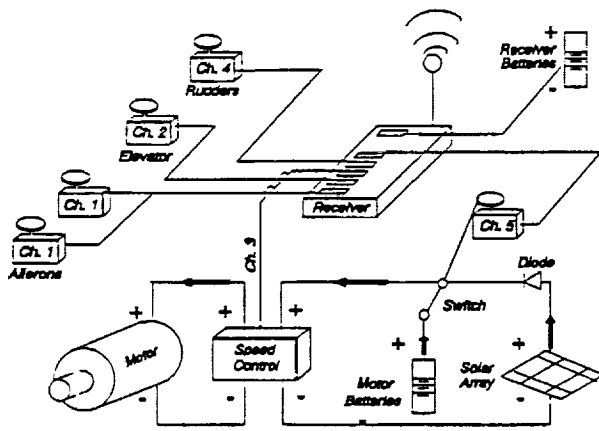


Fig. 5. Controls layout.

Controls and Interface

The modified remote control radio system and the necessary hardware for controlling deflecting surfaces and switches via servomotor, shown in Fig. 5, is the essence of the controls and interface scheme.

A propulsion powerplant divided into three subsections is employed. This system includes 98 solar cells, 7 rechargeable nickel-cadmium batteries, 1 DC motor, and 1 propeller, as shown in Fig. 5. This power circuit enables three modes of operation. In one mode the solar array is the sole source of input power. A second scenario occurs when the motor is turned off and the NiCad batteries are in parallel with the solar array: the array will charge the batteries provided the array has a high enough voltage and produces sufficient current. The option of using power from both the NiCad batteries and the solar array is also available.

The Sun is the only source of electrical input energy and the solar cells serve as the primary source of input power by converting the solar energy into electrical energy. The NiCad batteries serve as a safety feature, both as a secondary power source and a means of supplying short bursts of energy to the system when needed (i.e., for takeoff and critical maneuvers). The solar array and NiCad batteries are connected in parallel via a remotely controlled switch in series with the DC motor. The subsections were optimized to work together and the solar propulsion system was integrated into the final configuration.

Characteristics of solar cells were examined and several types of cells were considered. Finally, 12.5%, 3.75 x 3.75" cells were selected for the current design. The cells are of high quality and relatively good efficiency, yet their size and low power/weight ratio presents considerable constraints. The cells are placed within the wing and tail on foam supports. The supports are mounted on the rib sections to provide protection and maintain the aerodynamic quality of the configuration. Shading from the rib sections is inevitable. However, placing the cells as close as possible to the upper surface of the airfoil shape greatly alleviated this problem.

Decrease in transmittance caused by the mylar coating was theoretically and experimentally evaluated. Using the Fresnel

reflection equations⁽³⁾ and data provided by the cell manufacturer, the theoretical transmittance of the mylar coating was determined to be around 80%. Experimental evaluation yielded a transmittance of 90%.

A random sample of solar cells was tested on February 27, 1991, and the resulting current-voltage (I-V) and power curves were determined. A current adjustment was determined and applied to the experimental results. Voltage change as a function of both cell and ambient temperature was estimated⁽⁴⁾, taking into account the effect of light intensity. The ambient temperature for the test data was adjusted by +10° to account for the "greenhouse effect" within the wing. Applying the current and voltage adjustments to the experimental data, the I-V and power curves were estimated for a given flight date light intensity and current values (see Figs. 6 and 7). The Astro Cobalt 05 electric, geared motor and a two-bladed, folding propeller with a diameter of 33 cm and pitch of 16.5 cm manufactured by Aero-Haute were chosen for their combined efficiency. A combined contour plot of electrical input power, shaft torque, shaft RPM, and motor efficiency vs. voltage and current is shown in Fig. 8. Three motor-propeller combinations were tested in

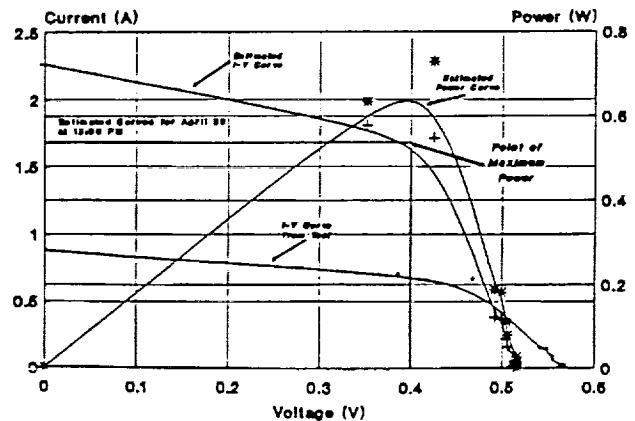


Fig. 6. Solar cell current-voltage curves.

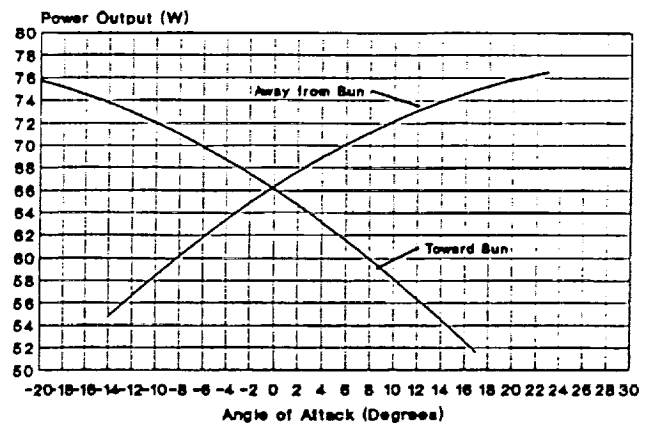


Fig. 7. Estimated power from solar cell curves.

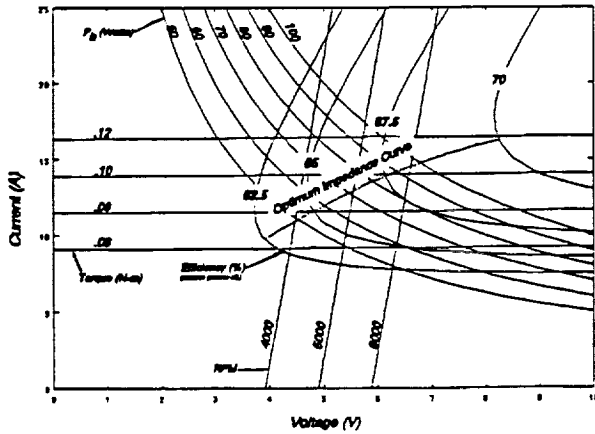


Fig. 8. Combined contour plot for design motor.

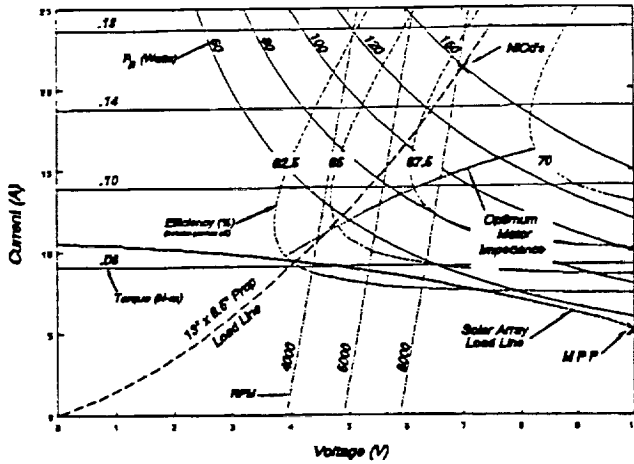


Fig. 9. Combined contour plot for design motor—Propeller setup.

the WPI wind tunnel under conditions similar to those in flight. Figure 9 illustrates the results of the tests performed for the chosen motor-propeller combination.

Stability

Longitudinal and lateral stability were evaluated by classical analysis methods⁽⁵⁾. The tail and support struts were sized to provide static longitudinal stability⁽⁶⁾. The effects of expected gust-induced loads in the longitudinal direction (pitch) results in a rate of change of the pitching moment with the total airplane lift of -0.1415, giving static stability to the configuration. In order to study the longitudinal dynamic stability of the configuration, the long- and short-period oscillatory modes of motions were examined. A second-order differential equation of the plane's motion was derived from Newton's second law and the damping ratio and natural frequency were determined. Results of the longitudinal dynamic stability analysis at the design point are given in Table 6.

TABLE 6. Dynamic longitudinal stability.

Motion	Frequency	Period
Long Period	0.948	2.12 s
Short Period	0.045	7.07 s

The vertical tail and dihedral were sized to provide lateral stability. The vertical tail has a volume coefficient of 0.018, which is very close to the typical value of 0.02 for a sailplane⁽⁷⁾, and furnishes directional stability. Dihedral stability is achieved by adding a small positive dihedral angle of 5° at a location of 0.75 m from the wing root, tending to return the aircraft to its equilibrium position once it has been disturbed by a rolling moment⁽⁷⁾.

Performance and Mode of Operation

Solar propulsion is very appealing because it is harmless to the environment and cost efficient. The performance of a vehicle, however, is very dependent on the weather, time of day, location, season, and efficiency of its solar-power system. The available solar cells for this aircraft configuration were not the most efficient or lightweight, yet did allow for excess power for takeoff and climb. A computer code was developed to predict the performance of the aircraft in level flight (see Fig. 10).

The aircraft is designed to climb in a circular flight path to an altitude of 50 m in 6.7 min, as shown in Fig. 11. This mission requires 7 complete revolutions about a 200-m field. The climb rate is a function of the angle of incidence between the Sun and the solar cell array; the aircraft climbs at a rate of 0.155 m/s away from the Sun and 0.093 toward the Sun.

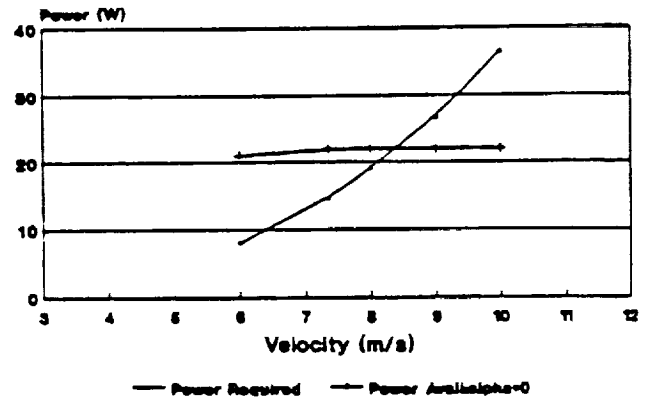


Fig. 10. Design power curve.

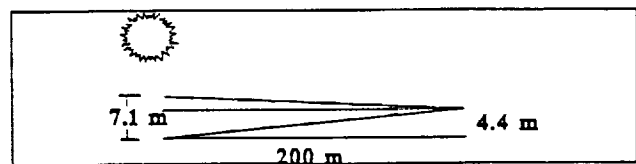


Fig. 11. Circular climb pattern.

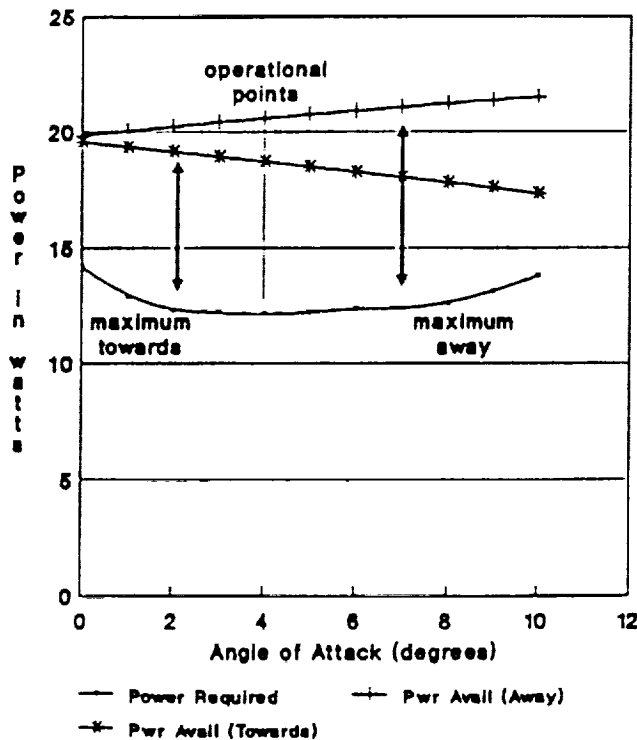


Fig. 12. Optimization of excess power with angle of attack.

At the design altitude, 15.9 W is required from the propulsion system to maintain flight at 7 m/s. A sustained figure-eight flight pattern will be achieved with an angle of attack of 4°, banking angle of 4°, and a turning radius of 79 m. Figure 12 shows the optimization of excess power with respect to the attack angle of the wing.

Construction Procedure

The final design of the solar-powered vehicle was meticulously constructed with every attempt to maintain the aerodynamic features and weight budget for each component and any additional items not initially allotted for. To facilitate transport, storage, and construction, modular features were incorporated into the final configuration. Consideration was given to the connections in order to maintain the structural integrity of the original design. Currently the aircraft is being prepared for a test flight to establish the effectiveness of the control system and its overall stability.

Environmental Impact

Society is faced with various self-induced environmental problems. Implementation of solar energy as a replacement to traditional energy resources provides an economical solution. The design and construction of this solar-powered aircraft attempts to contribute to this cause and encourage future research into alternative energy resources.

CONCLUSIONS

A preliminary study of a solar-powered MPRPV designed to operate at approximately sea level indicates that it is currently feasible to integrate solar propulsion into the design of airborne vehicles. Increased research on the potential of and possibilities for solar energy is encouraged.

ACKNOWLEDGMENTS

The assistance and technical support of the NASA contacts, WPI faculty, Mobil Solar, and many other interested aircraft modeling enthusiasts are very greatly appreciated. Special thanks to Art Glassman, our NASA/USRA mentor and the advising professors, Prof. William W. Durgin, Prof. Andreas N. Alexandrou, Prof. Ralph F. Cohn, Prof. Vahid Motevalli, Prof. David J. Olinger, Prof. Joseph J. Rencis, Prof. Clark, and Kurt Heinzmann for their faithful guidance. The educational assistance on low Reynolds number flight vital to the required mission provided by Don Harvey and Dan Somers, both affiliated with NASA Langley, has been invaluable. Also thanks to the many helpful students from WPI especially Adam Szymkiewicz, Jason Makofsky, and Kyle Jacobson for sharing their expertise.

REFERENCES

1. Selig, M., J. Donovan, and D. Fraser. 1989. *Soartech 8: Airfoils at Low Speeds*.
2. Eppler, R. and D. Somers. 1980. "A Computer Program for the Design and Analysis of Low-Speed Airfoils, Including Transition." NASA TM 80210.
3. Duffie, J. and W. Buckner. 1980. *Solar Engineering of Thermal Processes*. John Wiley and Sons, Inc., New York.
4. Buresch, M. 1983. *Photovoltaic Energy Systems: Design and Installation*. McGraw-Hill Inc., New York.
5. Nelson, R. 1989. *Flight Stability and Automatic Control*. McGraw-Hill. New York.
6. Shevell, R. 1983. *Fundamentals of Flight*. Prentice-Hall, Englewood Cliffs, New Jersey.
7. Raymer, D. 1989. *Aircraft Design: A Conceptual Approach*. American Institute of Aeronautics and Astronautics, Inc., Washington, D.C.

dmT

Space Projects

